Effects of Zonal Fields on Energetic-Particle Excitations of Reversed Shear Alfvén Eigenmode: Simulation and Theory

Liu Chen[1,2], Pengfei Liu[3,*], Ruirui Ma[4,2], Zhihong Lin[5], Zhiyong Qiu[6,2], Wenhao Wang[5], and Fulvio Zonca[2,1]

[1] *Institute for Fusion Theory and Simulation and School of Physics, Zhejiang University, Hangzhou, 310027, China*

[2] *Center for Nonlinear Plasma Science and C.R. ENEA Frascati, C.P. 65, 00044 Frascati, Italy*

[3] *Beijing National Laboratory for Condensed Matter Physics, CAS Key Laboratory of Soft Matter Physics, Institute of Physics, Chinese Academy of Sciences, Beijing 100190, China*

[4] *Southwestern Institute of Physics, P.O. Box 432, Chengdu, 610041, China*

[5] *Department of Physics and Astronomy, University of California, Irvine, CA 92697-4574, USA*

[6] *Institute of Plasma Physics, Chinese Academy of Sciences (ASIPP), Hefei 230031, China*

[*] *corresponding author. Email address: pfliu@iphy.ac.cn*

(Dated: October 18, 2024)

Employing both nonlinear gyrokinetic simulation and analytical theory, we have investigated the effects of zonal (electromagnetic) fields on the energetic particle's drive of reversed shear Alfvén eigenmodes in tokamak plasmas. Contrary to the conventional expectation, simulations with zonal fields turned on and off in the energetic particle dynamics while keeping the full nonlinear dynamics of the thermal plasma indicate that zonal fields further enhance the instability drive and lead, thus, to a higher saturation level. These puzzling simulation results can be understood analytically in terms of the general fishbone-like dispersion relation with the correspondingly different energetic-particle phase-space structures induced by the zonal fields. Analytical expressions for the zonal fields beat driven by the reversed shear Alfvén eigenmodes are also derived, and shown to be in good agreement with the simulation results.

PACS numbers: 52.30.Gz, 52.35.Bj, 52.35.Mw, 52.65.Tt

I. INTRODUCTION

The interaction between energetic particles (EPs) and Alfvén eigenmodes (AEs) is crucial for understanding the stability and transport dynamics of fusion plasmas in magnetic confinement devices; such as the tokamak. Among the various AEs, reversed shear Alfvén eigenmodes (RSAEs) [1, 2] have attracted significant interest due to their complex interplay with EPs in reversed shear configurations, which are essential for achieving self-organized steady-state operations conducive to sustained fusion. Previous extensive simulations on the nonlinear physics of RSAE [3–5] have clearly shown that the zonal electromagnetic fields (ZFs) could be beat driven by RSAE, and significantly lower the RSAE saturation level. There are two possible routes to achieve such suppression of RSAE by ZFs. The first route is via the nonlinear dynamics of thermal plasmas; such as nonlinear frequency shift and/or modification of the local current/safety factor profile; and thereby, enhance the continuum damping [4, 6]. The second route is via modifications by ZFs in the EP dynamics and drive. Studies on both routes have, so far, been qualitative, and underlying physics mechanisms remain not well understood. The focus of the present work is to investigate the physics of the second route up to the initial saturation.

More specifically, our aim is to provide, by using both nonlinear gyrokinetic simulation and theory, clear and detailed analyses on the nonlinear beat-driven generation of ZFs by RSAE, as well as how such ZFs affect the EP's drive of RSAE. To facilitate our analysis, we categorize our studies into three cases, referred to as cases A, B, and C; each representing different treatment of zonal fields in the EP dynamics. In Case A, labeled as "No-ZFs Case A", we focus on fully nonlinear thermal plasmas while deliberately excluding the effects of zonal fields on EPs. Case B, labeled as "Full-ZFs Case B", incorporates a fully nonlinear treatment of both thermal plasma and EPs; revealing the unexpected result that inclusion of the ZFs in EP dynamics yields an increased saturation level relative to the No-ZFs Case A. Lastly, Case C, labeled as "Partial-ZFs Case C", keeps fully nonlinear thermal plasmas, while removes zonal shearing effects in EPs; resulting in a negligible or, more precisely, a weak stabilizing effect on RSAE saturation when compared to the No-ZFs Case A. In all these three cases, we remark, ZFs are fully kept for the thermal ions and electrons.

Our findings indicate that including ZFs beat driven by RSAE in the EP dynamics tends to enhance EP's drive; resulting in a higher RSAE saturation level. More-over, suppressing zonal shearing effects in EPs appears to exert a stabilizing effect on the RSAE saturation level. These conclusions, contrary to conventional expectation, could be understood analytically in terms of the general fishbone-like dispersion relation [7, 8] with different EP phase-space zonal structures (PSZS) [9] generated in the three cases.

The paper is organized as follows: Section II presents the nonlinear simulation results from GTC [10] for the three cases discussed above. Section III presents analytical theories for the beat-driven zonal fields, as well as, for the three cases, EP PSZS generated by ZFs and their implications to RSAE stability. Conclusions and discussions are given in Sec. IV.

II. GTC SIMULATIONS

The equilibrium and plasma profiles adopted in GTC simulations [10] are selected from DIII-D discharge #159243 [11] at 805 ms and reproduced by with the kinetic EFIT code [12], which have also been well simulated in other benchmarking codes [3, 13]. The simulations employ a typical reversed magnetic shear configuration with minimal safety factor $q_{\min} = 2.94$ near major radius $R = 1.98$ m on the mid-plane for the low field side, where RSAE are observed in experiments and validated in simulations. Here, q, the safety factor, represents the ratio of toroidal to poloidal turns of magnetic field lines.

For the GTC simulation model [14], EP and thermal ions are described by gyrokinetic model [15], and electrons are described by drift kinetic model. Since $\beta \ll 1$ and $nq \gg 1$, the effects of compressible magnetic perturbation $\delta B_\parallel$ and equilibrium current $J_{\parallel 0}$ on RSAE, as verified in previous simulations, are negligible. Here β is the ratio between plasma and magnetic pressures, and n is the toroidal mode number. Using the parallel velocity, $v_\parallel$, description [15], the perturbed gyrokinetic Vlasov equation can be written as

$$(\mathcal{L}_0 + \delta\mathcal{L})\delta F = -\delta\mathcal{L} F_0, \qquad (1)$$

where F_0 is the equilibrium distribution, δF is the perturbed distribution, and the equilibrium and perturbed propagators in the $(\boldsymbol{X}, v_\parallel)$ phase space are given, respectively, by

$$\mathcal{L}_0 = \frac{\partial}{\partial t} + \left(v_\parallel \boldsymbol{b}_0 + \boldsymbol{v}_d\right) \cdot \frac{\partial}{\partial \boldsymbol{X}} - \frac{\mu \boldsymbol{B}_0^*}{B_0} \cdot \nabla B_0 \frac{\partial}{\partial v_\parallel}, \qquad (2)$$

and

$$\delta\mathcal{L} = \left(\boldsymbol{v}_E + \frac{v_\parallel \delta \boldsymbol{B}_\perp}{B_0}\right) \cdot \frac{\partial}{\partial \boldsymbol{X}} - \left(\frac{\mu \delta \boldsymbol{B}_\perp \cdot \nabla B_0}{B_0} + Z\frac{\boldsymbol{B}_0^*}{m B_0} \cdot \nabla\delta\phi + \frac{Z}{cm}\frac{\partial \delta A_\parallel}{\partial t}\right)\frac{\partial}{\partial v_\parallel}. \qquad (3)$$

Here, $\boldsymbol{X}$ is the gyro-center position, $\mu = v_\perp^2/2B_0$ is the magnetic moment, Z is the particle charge, m is the particle mass, c is the light speed, $\boldsymbol{B}_0$ is the equilibrium magnetic field, $\delta \boldsymbol{B}_\perp$ is the perpendicular magnetic perturbation, $\delta A_\parallel$ is the parallel component of the perturbed vector potential, and $\delta\phi$ is the perturbed scalar potential. Furthermore,

$$\boldsymbol{v}_d = \boldsymbol{b}_0 \times \left(\mu \boldsymbol{\nabla} B_0 + v_\parallel^2 \boldsymbol{\kappa}\right)/\Omega,$$

$$\boldsymbol{v}_E = \frac{c}{B_0}\boldsymbol{b}_0 \times \nabla\delta\phi,$$

$$\boldsymbol{B}_0^* = \boldsymbol{B}_0 + \frac{B_0 v_\parallel}{\Omega}\boldsymbol{b}_0 \times \boldsymbol{\kappa},$$

where $\boldsymbol{b}_0 = \boldsymbol{B}_0/B_0$, $\Omega = ZB_0/mc$, and $\boldsymbol{\kappa} = (\boldsymbol{b}_0 \cdot \boldsymbol{\nabla})\boldsymbol{b}_0$ being the curvature of $\boldsymbol{B}_0$. For a single n mode simulation with zonal components (labeled as subscript "z"), Eq. (1) can be further written as,

$$\left(\mathcal{L}_0 + \delta\mathcal{L}_n + \delta\mathcal{L}_z\right)\left(\delta F_n + \delta F_z\right) = -\left(\delta\mathcal{L}_n + \delta\mathcal{L}_z\right)F_0, \quad (4)$$

where $\delta\mathcal{L}_n$ and $\delta\mathcal{L}_z$ correspond to the perturbed propagators, Eq. (3), with, respectively, the toroidal mode number n and zonal components of the electromagnetic fields.

In GTC simulations, an initial Maxwellian distribution is used for thermal plasmas and EP with $T_e = T_i = 1$ keV and $T_E = 20$ keV. Simulations are performed using a low noise δf scheme [16] with a particle number per cell 1000 to minimize the noise. The radial boundary of the simulation domain is $R = [1.81, 2.23]$ m. Based on the convergence studies, GTC uses a global field-aligned mesh with 32 parallel grid points, which is sufficient to resolve the long parallel wavelength, and 5×10^4 unstructured perpendicular grid points with a grid size $\sim 1.3\rho_i$, where $\rho_i \sim 2.1$ mm is the thermal ion gyroradius. Time step is set to be 2×10^{-5} ms to resolve the high frequency RSAE and the fast electron thermal motion $v_{th,e} \sim 2\times10^7$ m/s. In addition, the initial condition is only random noise, and all poloidal harmonics are included for a select specific toroidal mode using Fourier filtering.

In the present work, in order to delineate the effects of zonal fields ($\delta\phi_z$, $\delta A_{\parallel z}$) on the EP dynamics, three cases of simulations, labeled as Case A, B, and C, are carried out for the most unstable $n = 4$ RSAE. Case A corresponds to the No-ZFs case, where we set $\delta\mathcal{L}_z = 0$ in the EP gyrokinetic Vlasov equation, Eq. (4), in order to remove the effects of ZFs on EP. Case B corresponds to the Full-ZFs case, where $\delta\mathcal{L}_z$ on both sides of Eq. (4) is kept for EP. Meanwhile, Case C corresponds to the Partial-ZFs case, where we keep $\delta\mathcal{L}_z$ in the right-hand side of Eq. (4); but we set $\delta\mathcal{L}_z = 0$ in the left-hand side of Eq. (4), i.e., the EP perturbed propagator, in order to remove the so-called shearing effects due to ZFs. Note that, in all three cases, ZFs are fully kept for the thermal electrons and ions.

Figure 1 (a) shows the time history of mode amplitude of $n = 4$ RSAE scalar potential, $\delta\phi_4$, for the three simulation cases. In the early linear phase, i.e., before 0.4 ms, effects of ZFs on the RSAE amplitude are negligible due to the small amplitude of ZFs. However, in the later linear phase, the Full-ZFs Case B, exhibits a stronger

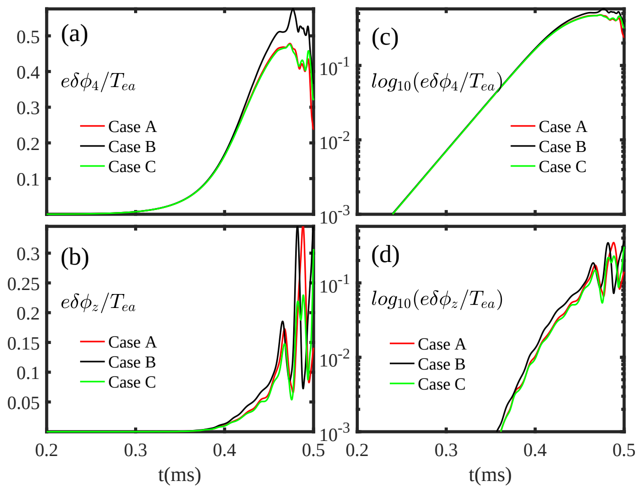

FIG. 1: Time history of perturbed electrostatic potential $e\delta\phi_4/T_{ea}$ (panel a), normalized by the on-axis electron temperature T_{ea}, for the selected toroidal $n = 4$ modes on $q_{\min}$ flux surface from Case A (red), B (black) and C (green). The normalized zonal scalar potential $e\delta\phi_z/T_{ea}$ (panel b) is the root-mean-square (rms) value averaged over the radial domain of the major radius $R = [1.91, 2.04]$ m. Panel (c) and (d) are the corresponding plots using a base-10 logarithmic scale on the vertical axis.

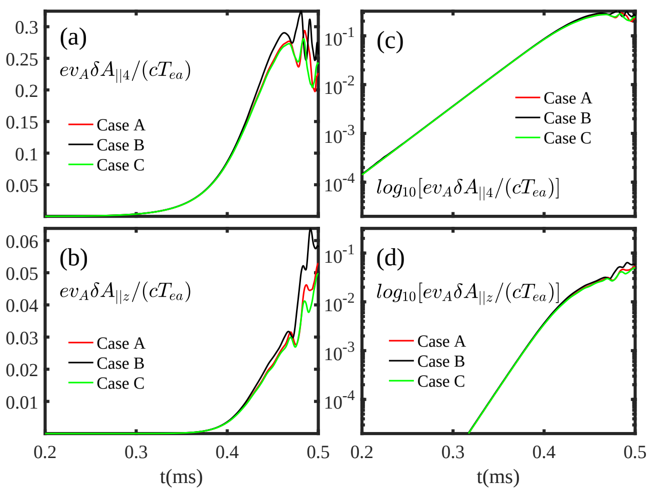

FIG. 2: Time history of parallel vector potential $ev_A\delta A_{\|4}/(cT_{ea})$ (panel a), normalized by the on-axis electron temperature T_{ea} and Alfvén speed $v_A = B_a/\sqrt{4\pi n_{ea} m_i}$ with the ion mass m_i, the on-axis magnetic field B_a and ion density n_{ea}. Panel (b) displays the time history of normalized zonal vector potential $ev_A\delta A_{\|z}/(cT_{ea})$. Panel (c) and (d) are the corresponding plots using a base-10 logarithmic scale on the vertical axis.

drive and, thereby, a higher initial saturation level than the No-ZFs Case A and Partial-ZFs Case C. This result contradicts with the conventional expectation that ZFs tend to suppress instabilities and, thereby, lower the saturation level. Furthermore, that the No-ZFs Case A essentially overlaps with the Partial-ZFs Case C is also puzzling; since it suggests that $\delta\mathcal{L}_z$ in the right-hand side of Eq. (4) has a negligible effect on RSAE excitations by EP. It is worthwhile noting that the effects of ZFs also enter implicitly via the PSZS, δF_z, which cannot be suppressed in simulations. Consequently, as will be demonstrated in Sec. III B, these puzzling simulation results could be understood analytically employing the GFLDR along with the different EP PSZS nonlinearly generated in the three cases. Figure 1 (b), meanwhile, plots the time history of the nonlinearly generated zonal potentials, $\delta\phi_z$, for the three cases. Curves for $e\delta\phi_4/T_{ea}$ and $e\delta\phi_z/T_{ea}$ are also plotted in Figs. 1 (c) and (d) in semi-log scale. During the linear phase, it is observed, as in previous RSAE simulations, that the ZFs grow at twice the linear growth rate of RSAE; clearly indicating that the ZFs are beat driven by RSAE [3, 5, 17]. Figure 2 plots the corresponding time histories of the parallel vector potential, $\delta A_\|$; showing the same features as $\delta\phi$. Adopting the beat driven generating mechanism, we will derive in the Sec. III A the corresponding analytical expressions of $\delta\phi_z$ and $\delta A_{\|,z}$; which are shown to be in good agreement with simulations, and used later in Sec. III B to analyze effects of ZFs on EP excitations.

III. THEORETICAL ANALYSIS

A. Beat-driven zonal electromagnetic fields by RSAE

Let us consider a large aspect-ratio tokamak with circular magnetic surfaces; i.e., $\epsilon \equiv r/R \sim \mathcal{O}(10^{-1}) < 1$ with r and R being, respectively, the minor and major radii. β, meanwhile, is taken to be $\mathcal{O}(\epsilon^2) \ll 1$. Let $\Omega_0 = (\omega_0, n_0)$ denote a RSAE with toroidal mode number n_0 and mode frequency $\omega_0 = \omega_{0r} + i\partial_t$. Note Ω_0 could be either linearly excited by EPs with $\partial_t = \gamma_0 \ll \omega_{0r}$ being the linear growth rate, or excited by an external antenna with $\partial_t \to 0^+$. Since $\beta \ll 1$, magnetic compression is negligible and, thus, Ω_0 is described by electromagnetic perturbations; $\delta\phi_0$ and $\delta A_{\|0}$ with $\delta\phi_0$ and $\delta A_{\|0}$ being the scalar and parallel vector potentials, respectively. More specifically, we take

$$\begin{pmatrix} \delta\phi_0 \\ \delta A_{\|0} \end{pmatrix} = e^{-i\omega_{0r}t + in_0\xi} \sum_m \begin{pmatrix} \Phi_m(r,t) \\ A_m(r,t) \end{pmatrix} e^{-im\theta} + \text{c.c.} \quad (5)$$

Here, ξ is the toroidal angle and θ the poloidal angle. Since $|k_{\perp 0}\rho_i|^2 \ll 1$ with $k_{\perp 0}$ being the perpendicular wave vector for Ω_0, we may further assume Ω_0 satisfying the ideal MHD approximation; $\delta E_{\|0} \simeq 0$; i.e., $\omega_0 \delta A_{\|0} =$

$-ic(\boldsymbol{b}_0\cdot\nabla)\delta\phi_0$, or

$$k_{\parallel m}\Phi_m=\omega_0 A_m/c, \tag{6}$$

where $k_{\parallel m}=(n_0q-m)/qR$.

We now consider the nonlinear generation of the zero-frequency ZFs beat driven by Ω_0. Let the corresponding zonal state be denoted as $\Omega_z=(\omega_z,n=0)$; that is,

$$\begin{pmatrix}\delta\phi_z\\ \delta A_{\parallel z}\end{pmatrix}=\begin{pmatrix}\Phi_z(r,t)\\ A_z(r,t)\end{pmatrix}+\text{c.c.}, \tag{7}$$

and $|-i\omega_z|=|\partial_t\ln\Phi_z|=|\partial_t\ln A_z|\ll\omega_{bi},\,\omega_{ti},\,\omega_{0r}$ with ω_{bi} and ω_{ti} being, respectively, the thermal ion bounce and transit frequencies. The governing equation, first, is the nonlinear gyrokinetic equation [18] for the non-adiabatic component of the perturbed distribution function, δg_j, given, for $j=$ species, by

$$\left[\mathcal{L}_g\delta g_j\right]_k=i\left(\frac{e}{m}\right)_j QF_{0j}\langle\delta L_k\rangle-\left[\langle\delta\boldsymbol{U}_g\rangle\cdot\boldsymbol{\nabla}\delta g_j\right]_k, \tag{8}$$

where

$$\mathcal{L}_g=\partial_t+v_\parallel\boldsymbol{b}_0\cdot\boldsymbol{\nabla}+\boldsymbol{v}_d\cdot\boldsymbol{\nabla}, \tag{9}$$

$$QF_{0j}=(i\partial_t\partial/\partial\varepsilon+\hat{\omega}_{*k})F_{0j}, \tag{10}$$

$$\hat{\omega}_{*k}F_{0j}=-i(\boldsymbol{b}_0/\Omega_j\times\boldsymbol{\nabla}F_{0j})\cdot\boldsymbol{\nabla}, \tag{11}$$

and $\delta L_k=(\delta\phi-v_\parallel\delta A_\parallel/c)_k$. Meanwhile, $\varepsilon=v^2/2$, $\langle A\rangle$ denotes the gyro-averaged A; i.e., $\langle\delta L_k\rangle=J_k\delta L_k$ with $J_k=J_0(\lambda_{kj})$, J_0 being the Bessel function, $\lambda_{kj}=k_\perp\rho_j$, and $\rho_j=v_\perp/\Omega_j$. Note here that the wave vector, $\boldsymbol{k}$, should, in general, be understood as an operator, $\boldsymbol{k}=-i\boldsymbol{\nabla}$. Finally, noting

$$\begin{aligned}\langle\delta\boldsymbol{U}_g\rangle_k&=\langle\delta\boldsymbol{U}_E\rangle+v_\parallel\langle\delta\boldsymbol{B}_\perp\rangle/B_0\\&=\frac{c}{B_0}\boldsymbol{b}_0\times\boldsymbol{\nabla}\langle\delta L_k\rangle,\end{aligned} \tag{12}$$

the nonlinear term can then be expressed in terms of the wave vectors as

$$\left[\langle\delta\boldsymbol{U}_g\rangle\cdot\boldsymbol{\nabla}\delta g\right]_k=\left(\frac{c}{B_0}\right)\Lambda^{k'}_{k''}\left[\langle\delta L_{k'}\rangle\delta g_{k''}\right], \tag{13}$$

where $\boldsymbol{k}'+\boldsymbol{k}''=\boldsymbol{k}$, and

$$\Lambda^{k'}_{k''}\equiv(c/B_0)(\boldsymbol{k}''_\perp\times\boldsymbol{k}'_\perp)\cdot\boldsymbol{b}_0. \tag{14}$$

Note also, since $n_{EP}/n_b\ll 1$, the EP contribution to the ZFs is, typically, negligible.

To generate the ZFs, let us first consider the electron responses. Letting $\delta g_{ze}=\delta g^{(1)}_{ze}+\delta g^{(2)}_{ze}$, we then have, from Eq. (8) and noting $|k_\perp\rho_e|\lesssim|k_\perp\rho_{be}|\ll 1$, for trapped electrons,

$$\delta g^{(1)}_{ze,t}=-\frac{e}{T_e}F_{Me}\delta\phi_z, \tag{15}$$

and, for circulating electrons,

$$\delta g^{(1)}_{ze,c}=-\frac{e}{T_e}F_{Me}(\delta\phi-\bar{v}_\parallel\delta A_\parallel/c)_z. \tag{16}$$

In deriving Eqs. (15) and (16), we have taken the thermal plasma to be Maxwellian, and $\bar{v}_\parallel$ is the transit-averaged $v_\parallel$. For the nonlinear response, $\delta g^{(2)}_{ze}$, meanwhile, we have, from Eq. (8),

$$\begin{aligned}\left[(\partial/\partial t+v_\parallel\boldsymbol{b}_0\cdot\boldsymbol{\nabla})\delta g^{(2)}_e\right]_z=-\frac{c}{B_0}\Big[\Lambda^{k'}_{k''}\Big(&\delta\phi\\&-\frac{v_\parallel\delta A_\parallel}{c}\Big)_{k'}\delta g_{k''}\Big]_z.\end{aligned} \tag{17}$$

Noting that, for RSAE, $|k_\parallel v_{te}|\gg|\omega_k|$, we have, from Eq. (8),

$$\delta g_{k'e}\simeq\delta g^{(1)}_{k'e}\simeq-\frac{e}{T_e}F_{Me}\left(1-\frac{\omega_{*e}}{\omega}\right)_{k'}\delta\psi_{k'}. \tag{18}$$

Here, $\omega_{*jk}=\omega_{*jn}[1+\eta(v^2/v_t^2-3/2)]_j$ with $\omega_{*jn}=(cT/eB_0)_j(\boldsymbol{k}\times\boldsymbol{b}_0)\cdot\boldsymbol{\nabla}\ln N_j$ and $\eta_j=|\nabla T_j|/|\nabla N_j|$, and $\delta\psi_{k'}=(\omega\delta A_\parallel/ck_\parallel)_{k'}=\delta\phi_{k'}$ via the ideal MHD constraint, Eq. (6). Equation (17) then readily yields, for the trapped electrons,

$$\delta g^{(2)}_{ze,t}\simeq\frac{c}{B_0}\frac{e}{T_e}F_{Me}\frac{1}{\omega^2_{k'r}}\frac{\partial}{\partial r}\left[(k_\theta\omega_{*e})_{k'}\delta\phi_{k'}\delta\phi_{k''}\right]_z, \tag{19}$$

and, for the circulating electrons,

$$\delta g^{(2)}_{ze,c}\simeq\frac{c}{B_0}\frac{e}{T_e}F_{Me}\frac{1}{\omega^2_{k'r}}\frac{\partial}{\partial r}\left[\left(k_\theta\omega_{*e}-\bar{v}_\parallel k_\theta k_\parallel\right)_{k'}\delta\phi_{k'}\delta\phi_{k''}\right]_z. \tag{20}$$

In deriving Eqs. (19) and (20), we have noted $\boldsymbol{k}'=k_{\theta 0}\hat{\boldsymbol{\theta}}+k_{\parallel 0}\boldsymbol{b}_0-i\hat{\boldsymbol{r}}\partial/\partial r$, $\boldsymbol{k}''=-k_{\theta 0}\hat{\boldsymbol{\theta}}-k_{\parallel 0}\boldsymbol{b}_0-i\hat{\boldsymbol{r}}\partial/\partial r$, $\omega_{k'}=\omega_{0r}+i\partial/\partial t$, and $\omega_{k''}=-\omega_{0r}+i\partial/\partial t$. Also, noting Eq. (5), $[\delta\phi_{k'}\delta\phi_{k''}]_z=|\delta\phi_0|^2$ should be understood as summing up all the poloidal harmonics; e.g.

$$\left[\left(k_\theta k_\parallel\right)_{k'}\delta\phi_{k'}\delta\phi_{k''}\right]_z=\sum_m\frac{n_0q}{r}\frac{(n_0q-m)}{qR}\left|\Phi_m(r)\right|^2. \tag{21}$$

For ions, however, we need, in general, to keep the finite Larmor-radius and drift-orbit-width effects via the transformation to the drift/banana centers [19]. That is, letting

$$\delta g_{zi}=\exp(-i\lambda_{di})\delta g_{zid}, \tag{22}$$

where $\lambda_{di}=k_{zr}\rho_{dr}$, $v_\parallel\partial_l\rho_{dr}=v_{dr}$, and following steps essentially the same as those for electrons, we then derive from Eqs. (8)-(13), $\delta g_{zid}=\delta g^{(1)}_{zid}+\delta g^{(2)}_{zid}$. Here, for trapped ions,

$$\delta g^{(1)}_{zid,t}\simeq\left(\frac{e}{T_i}F_{Mi}\right)J_z\left(\mathcal{J}_{z0}\delta\phi-\mathcal{J}_{z1}\delta A_\parallel\right)_z, \tag{23}$$

and, for circulating ions,

$$\delta g^{(1)}_{zid,c} \simeq \left(\frac{e}{T_i}F_{Mi}\right) \mathcal{J}_{z0} J_z \left(\delta\phi - \bar{v}_\parallel \delta A_\parallel/c\right)_z . \quad (24)$$

In Eqs. (23) and (24), $\mathcal{J}_{z0} = \overline{\exp(i\lambda_{di})}$ and $\mathcal{J}_{z1} = \overline{(v_\parallel/c)\exp(i\lambda_{di})}$ correspond to finite drift-orbit/banana-width effects, and $\overline{(...)}$ denotes bounce averaging. Meanwhile, $\delta g^{(2)}_{zid}$, is given, for both trapped and circulating, ions, approximately by

$$\delta g^{(2)}_{zid} \simeq -\frac{c}{B_0}\frac{e}{T_i}\frac{F_{Mi}}{\omega^2_{0r}}\mathcal{J}_{z0}\frac{\partial}{\partial r}\left[J^2_{k'}k'_\theta\omega_{*k'}\delta\phi_{k'}\delta\phi_{k''}\right]_z . \quad (25)$$

Here, again, $[\cdots]_z$ should be understood as summing over all the poloidal harmonics. We note that, in deriving Eq. (25), we have ignored the ion $(v_\parallel\delta A_\parallel/c)_k$ contributions from RSAE, since $|\omega_k| \gg |k_\parallel v_{ti}|$. Equations (22)-(25) then yield

$$\delta g^{(1)}_{zi,t} \simeq \left(\frac{eF_{Mi}}{T_i}\right) J_z\mathcal{J}_{z0}\left(\mathcal{J}_{z0}\delta\phi - \mathcal{J}_{z1}\delta A_\parallel\right)_z , \quad (26)$$

$$\delta g^{(1)}_{zi,c} \simeq \left(\frac{eF_{Mi}}{T_i}\right) \mathcal{J}^2_{z0} J_z \left(\delta\phi - \bar{v}_\parallel\delta A_\parallel/c\right)_z , \quad (27)$$

and

$$\delta g^{(2)}_{zi} \simeq -\frac{c}{B_0}\frac{e}{T_i}\frac{F_{Mi}}{\omega^2_{0r}}\mathcal{J}^2_{z0}J^2_0\frac{\partial}{\partial r}\left[k_{\theta 0}\omega_{*i0}\left|\delta\phi_0\right|^2\right] . \quad (28)$$

With the δg_z's derived, we can then proceed to calculate $\delta\phi_z$ and $\delta A_{\parallel z}$. First, the parallel Ampère's law, $\nabla^2_\perp\delta A_{\parallel z} = 4\pi\delta J_z/c$, can be readily shown to yield

$$\begin{aligned}\frac{A_z}{c} &\simeq \frac{c}{B_0\omega^2_{0r}}\frac{\partial}{\partial r}\left[k_{\theta 0}k_{\parallel 0}|\delta\phi_0|^2\right] \\ &= \frac{c}{B_0\omega^2_{0r}}\frac{\partial}{\partial r}\sum_m\left(\frac{n_0 q}{r}\right)\frac{(n_0 q - m)}{qR}\left|\Phi_m\right|^2 .\end{aligned} \quad (29)$$

In deriving Eq. (29), we have noted that $\delta J_z \simeq \delta J_{ze}$ since $m_i \gg m_e$, $|\nabla_\perp c/\omega_{pe}|^2 \ll 1$, and Eq. (21). Next the quasi-neutrality condition for the Ω_z zonal mode; taking single charged ions and $\tau = T_e/T_i$,

$$\frac{N_i e^2}{T_e}(1+\tau)\delta\phi_z = \sum_{j=e,i} e_j\langle J_z\delta g_{zj}\rangle_v , \quad (30)$$

then yields

$$\begin{aligned}\Phi_z &\simeq \frac{c}{B_0}\frac{1}{\omega^2_{0r}}(1+c_0\eta_i)\partial_r\left[k_{\theta 0}\omega_{*in}|\delta\phi_0|^2\right] , \\ &= \frac{c}{B_0\omega^2_{0r}}(1+c_0\eta_i)\frac{\partial}{\partial r}\sum_m\left(\frac{n_0 q}{r}\right)\omega_{*in}\left|\Phi_m\right|^2 .\end{aligned} \quad (31)$$

where

$$c_0 = \langle(1-\mathcal{J}^2_{z0})(v^2/2v^2_{ti}-3/2)F_{Mi}\rangle_v / \langle(1-\mathcal{J}^2_{z0})F_{Mi}\rangle_v , \quad (32)$$

and we have taken $J^2_z \simeq J^2_0 \simeq 1$ but kept $\mathcal{J}^2_{z0}$. Note that, for $|\lambda_{di}| < 1$, $\langle(1-\mathcal{J}^2_{z0})F_{Mi}\rangle_v$ corresponds to the Rosenbluth-Hinton neoclassical polarization due to the trapped ions [20], and $c_0 \simeq 1$. In deriving Eq. (31), we have noted that, from Eq. (29) and $|n_0 q_{\min} - m| \ll 1$ for RSAE, the $\mathcal{J}_{z1}\delta A_{\parallel z}$ term due to trapped ions in Eq. (23) generally makes negligible contribution to $\delta\phi_z$. Equations (29) and (31), thus, correspond to the zonal electromagnetic fields, ZFs, beat driven by the ponderomotive force of the RSAE, Ω_0.

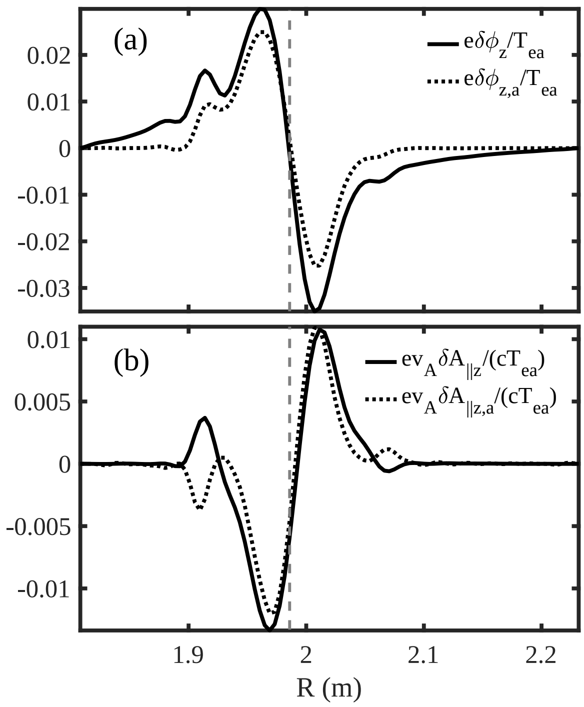

FIG. 3: Radial profiles of normalized zonal scalar potential $\delta\phi_z$ from the Full-ZFs Case B (solid line) and the analytically derived $\delta\phi_z$ using Eq. (31) with $c_0 = 1$ (dot dash line) on the mid-plane for the low field side at $t = 0.42$ ms [panel (a)]. The radial profiles of corresponding normalized zonal parallel vector potential $\delta A_{\parallel z}$ using Eq. (29) are shown in panel (b). The gray dash lines represent the $q_{\min}$ flux surface.

To compare the analytical expression with simulation results, we have plotted (black solid line) in Fig. 3 (a) the radial profile of normalized $\delta\phi_z$ from the Full-ZFs Case B simulation at $t = 0.42$ ms linear phase. The black dash line, meanwhile, is the corresponding analytical curve according to Eq. (31) with $c_0 = 1$. Similar curves for $\delta A_{\parallel z}$ with Eq. (29) are plotted in Fig. 3 (b). It can be observed that the analytical and simulation results are in good agreement for both zonal fields. It, thus, gives us confidence in employing the analytical expressions to investigate effects of ZFs on EP excitation in Sec. III B. We remark that the expressions for A_z and Φ_z given, respectively, by Eqs. (29) and (31) are derived subject to a minimal of approximations and, thus, can be expected to be also generally valid for other types of high-frequency AEs; e.g., the toroidal Alfvén eigenmode (TAE) [21].

B. Energetic-particle excitations of RSAE and phase-space zonal structures

To analyze how ZFs affect the EP drive on RSAE, we first note that, with $\delta\phi_0 = \delta\psi_0$, the corresponding gyrokinetic vorticity equation can be written as [22]

$$B_0\left(\partial_t+\frac{\delta\boldsymbol{B}_\perp}{B_0}\cdot\boldsymbol{\nabla}\right)\left(\frac{\delta J_\parallel}{B_0}\right)-\boldsymbol{\nabla}\cdot\sum\left\langle\left(\frac{e^2}{m}\frac{2\mu}{\Omega^2}B_0\partial_\varepsilon F_{0j}\right)\left(\frac{J_0^2-1}{\lambda^2}\right)\right\rangle_v\boldsymbol{\nabla}_\perp\partial_t\delta\phi-\sum ec\boldsymbol{b}_0\times\boldsymbol{\nabla}\left\langle\frac{2\mu}{\Omega}F_{0j}\left(\frac{J_0^2-1}{\lambda^2}\right)\right\rangle_v \cdot\boldsymbol{\nabla}\nabla_\perp^2\delta\phi+\sum e\boldsymbol{\nabla}_\perp\cdot\langle\boldsymbol{v}_d J_0\delta g_j\rangle_v+\delta\boldsymbol{B}_\perp\cdot\boldsymbol{\nabla}\left(\frac{J_{\parallel 0}}{B_0}\right) +\sum e\left\langle J_0\left[\frac{c}{B_0}\boldsymbol{b}_0\times\boldsymbol{\nabla}(J_0\delta\phi)\cdot\boldsymbol{\nabla}\delta g_j\right]\right\rangle_v=0. \tag{33}$$

In Eq. (33), $\sum$ is over all j = species, and we have assumed F_{0j} is isotropic; $\partial F_{0j}/\partial\mu = 0$. From Eq. (33), we can then derive variationally a general fishbone-like dispersion relation (GFLDR) [7, 8] and extract the following EP contribution to the RSAE instability drive;

$$\mathbb{I}\mathrm{m}\delta W_{k0} \equiv e_E\mathbb{I}\mathrm{m}\int d^3\boldsymbol{X}\left\{\delta\phi_0^*\left\langle\left(J_0\omega_z+\omega_d J_0\right)\delta g_{E0}\right\rangle_v\right\}. \tag{34}$$

Here, $\omega_z = -i\langle\delta\boldsymbol{U}_g\rangle_z\cdot\boldsymbol{\nabla}_\perp$, $\omega_d = -i\boldsymbol{v}_d\cdot\boldsymbol{\nabla}_\perp$, and $\mathbb{I}\mathrm{m}$ denotes the imaginary part due to wave-particle resonance, and $\mathbb{I}\mathrm{m}\delta W_{k0} > 0$ gives rise to instability drive. Note that, as observed in simulations [3, 23–25], $|\langle\delta\boldsymbol{U}_g\rangle_z\cdot\boldsymbol{\nabla}_\perp|$ is, typically, of $\mathcal{O}(\gamma_L) \ll |\boldsymbol{v}_{dE}\cdot\boldsymbol{\nabla}_\perp|$. Thus, ZFs effects on $\mathbb{I}\mathrm{m}\delta W_{k0}$ predominantly enter via δg_{E0}. To understand the simulation results in terms of the above analytical theory; i.e., Eq. (34), we need to establish the connection between the perturbed distribution functions obtained in simulation and δg.

First, we note that, in simulations, one employs the gyro-center distribution function; i.e.,

$$f = \left(\frac{e}{m}\right)\frac{\partial F_0}{\partial\varepsilon}\left(1-e^{-\boldsymbol{\rho}\cdot\boldsymbol{\nabla}}J_0\right)\delta\phi + e^{-\boldsymbol{\rho}\cdot\boldsymbol{\nabla}}f_g, \tag{35}$$

where f_g satisfies the following nonlinear gyro-center gyrokinetic equation [15]

$$\left(\mathcal{L}_g+\delta\mathcal{L}_X+\delta\mathcal{L}_\varepsilon\right)f_g = 0, \tag{36}$$

$\mathcal{L}_g$ is given by Eq. (9), $\delta\mathcal{L}_X = \langle\delta\boldsymbol{U}_g\rangle\cdot\boldsymbol{\nabla}$, $\langle\delta\boldsymbol{U}_g\rangle$ is given by Eq. (12), $\delta\mathcal{L}_\varepsilon = \delta\dot{\varepsilon}\partial/\partial\varepsilon$, and

$$\delta\dot{\varepsilon} = \left(\frac{e}{m}\right)\left[v_\parallel\left(\boldsymbol{b}_0+\frac{\langle\delta\boldsymbol{B}_\perp\rangle}{B_0}\right)\cdot\langle\delta\boldsymbol{E}\rangle+\boldsymbol{v}_d\cdot\langle\delta\boldsymbol{E}\rangle\right]. \tag{37}$$

Note that, in Eq. (36), in order to facilitate the connection with δg, we employ the $\varepsilon = v^2/2$ variable instead of the equivalent Eq. (1) in terms of the $v_\parallel$ variable. In analytical theory [18], we have

$$f = F_0+\left(\frac{e}{m}\right)\frac{\partial F_0}{\partial\varepsilon}\delta\phi + e^{-\boldsymbol{\rho}\cdot\boldsymbol{\nabla}}\delta g. \tag{38}$$

Thus, letting $f_g = F_{g0}+\delta F_g$, noting $F_0 = \exp(-\boldsymbol{\rho}\cdot\boldsymbol{\nabla})F_{g0}$, we then readily obtain

$$\delta g = \delta F_g - \left(\frac{e}{m}\right)\frac{\partial F_{g0}}{\partial\varepsilon}J_0\delta\phi. \tag{39}$$

We remark that the two nonlinear gyrokinetic equations, Eqs. (8) and (36), are the same except in Eq. (8) we have ignored the $\mathcal{O}(\rho/R)$ higher-order small terms due to the so-called parallel nonlinearities.

Let us consider simulations where only one single-n_0 RSAE ($\delta\phi_0$, $\delta A_{\parallel 0}$) and ZFs ($\delta\phi_z$, $\delta A_{\parallel z}$) are kept. Thus, letting, correspondingly, $\delta F_g = \delta F_{g0}+\delta F_{gz}$, Eq. (36) then yields, for the Ω_0 RSAE perturbation,

$$\left(\mathcal{L}_g+\delta\mathcal{L}_{zX}+\delta\mathcal{L}_{z\varepsilon}\right)\delta F_{g0} = -\left(\delta\mathcal{L}_{0X}+\delta\mathcal{L}_{0\varepsilon}\right)\left(F_{g0}+\delta F_{gz}\right). \tag{40}$$

Meanwhile, for the Ω_z zonal perturbation, we have

$$\mathcal{L}_g\delta F_{gz} \simeq -\delta\mathcal{L}_{z\varepsilon}F_{g0}-\left[\delta\mathcal{L}_{0X}\delta F_{g0}\right]_z. \tag{41}$$

In deriving Eq. (41) we have noted $\delta\mathcal{L}_{zX}(\delta F_{gz}, F_{g0}) = 0$, and neglected the small corrections of $\delta\mathcal{L}_{z\varepsilon}\delta F_{gz}$ as well as $\delta\mathcal{L}_{0\varepsilon}\delta F_{g0}$ relative to, respectively, $\delta\mathcal{L}_{z\varepsilon}F_{g0}$ and $\delta\mathcal{L}_{0X}\delta F_{g0}$.

We now proceed to analyze, for the three simulation cases presented in Sec. II, the corresponding δg_E and stability properties. From now on, we will, unless necessary, drop the subscript E in order to simplify the notations.

(Case A) No ZFs in EP. In this case, $\delta\phi_z = \delta A_{\parallel z} = 0$ and Eq. (40) becomes

$$\mathcal{L}_g\delta F_{g0A} = -(\delta\mathcal{L}_{0X}+\delta\mathcal{L}_{0\varepsilon})(F_{g0}+\delta g_{zA}). \tag{42}$$

Here, we have noted, from Eq. (39), $\delta F_{gzA} = \delta g_{zA}$. Also, using Eq. (39) for δF_{g0} and noting Eq. (9), Eq. (42) further reduces to

$$\begin{aligned}\mathcal{L}_g\delta g_{0A} &= i\left(\frac{e}{m}\right)\omega_{0r}\frac{\partial F_{g0}}{\partial\varepsilon}J_0\left(\delta\phi-\frac{v_\parallel\delta A_\parallel}{c}\right)_0 \\ &\quad -\delta\mathcal{L}_{0X}\left(F_{g0}+\delta g_{zA}\right)_0 \\ &\simeq i\left(\frac{e}{m}\right)Q(F_{g0}+\delta g_{zA})J_0\left(\delta\phi-\frac{v_\parallel\delta A_\parallel}{c}\right)_0.\end{aligned} \tag{43}$$

In Eq. (42), we have approximated $\partial_\varepsilon F_{g0} \simeq \partial_\varepsilon(F_{g0}+\delta g_{zA})$. δg_{zA}, meanwhile, is given by Eq. (41); i.e.,

$$\begin{aligned}\mathcal{L}_g\delta g_{zA} &= -\left[\delta\mathcal{L}_{0X}\delta g_{0A}\right]_z \\ &= -\left[\langle\delta\boldsymbol{U}_g\rangle_0\cdot\boldsymbol{\nabla}\delta g_{0A}\right]_z.\end{aligned} \tag{44}$$

Equation (44) shows that, in the present case of no ZFs, the phase-space zonal structure is, as expected, generated only by the symmetry-breaking Ω_0 RSAE fluctuations. Equations (43) and (44), thus, correspond to the single-wave model [26] and have been extensively studied in the literature [25, 27–34] and can be cast in a Dyson-like equation [9, 22]. We, furthermore, remark that, in Eq. (43), $\delta\mathcal{L}_{0x}F_{g0} = \langle\delta\boldsymbol{U}_g\rangle_0 \cdot \boldsymbol{\nabla} F_{g0}$ provides the expansion free energy for the linear instability drive. δg_{zA}, meanwhile, gives rise to the clump-hole structure near the wave-particle resonance and, thereby, reduces the instability drive near the peak of the RSAE; resulting in a net stabilizing effect [35, 36]. This feature can be clearly observed in Fig. 4 where δF_z is plotted in the (ε, R) phase space for $\mu B_a = 80$ keV at $t = 0.42$ ms linear phase in the Case A simulation.

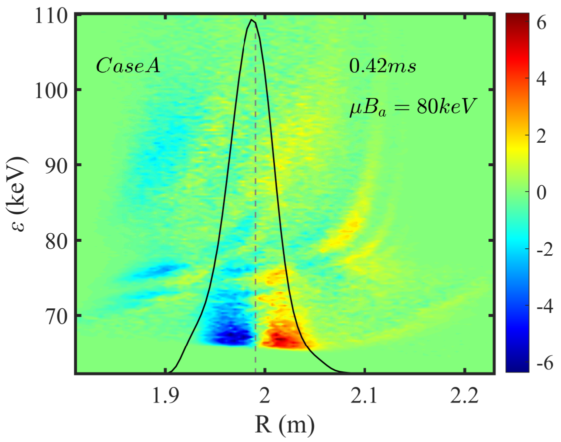

FIG. 4: Perturbed EP zonal distribution function δF_z with fixed $\mu B_a = 80$ keV in (ε, R) phase space taken at 0.42 ms in the linear phase of Case A simulation. The black lines represent the radial structure of RSAE intensity $|\delta\phi_4|^2$, and the gray dash line represents the $q_{\min}$ location.

To be more specific, we follow the linear gyrokinetic theory [37] and let

$$\delta g_{0A} = -\left(\frac{e}{m}\right)\left(\frac{Q}{\omega_{0r}}\right)(F_0 + \delta g_{zA})\, J_0\delta\Psi_0 + \delta K_{0A}, \quad (45)$$

Equation (43), with $\delta\phi_0 = \delta\psi_0$, then leads to

$$\mathcal{L}_g\delta K_{0A} = i\left(\frac{e}{m}\right) J_0\frac{\omega_d}{\omega_{0r}}\delta\phi_0 Q(F_0 + \delta g_{zA}). \quad (46)$$

$\mathbb{I}\mathrm{m}\delta W_{k0}$, Eq. (34), meanwhile, becomes

$$\mathbb{I}\mathrm{m}\delta W_{k0A} = e_E\mathbb{I}\mathrm{m}\int d^3\boldsymbol{X}\left\{\delta\phi_0^*\left\langle\omega_d J_0\delta K_{0A}\right\rangle_v\right\}. \quad (47)$$

To proceed further analytically and, thereby, illuminate the underlying physics more clearly, let us further simplify the analysis by considering only trapped EPs. Taking $\omega_{bE} \gg |\omega_0|, |\omega_d|$, we then have

$$\delta K_{0A} \simeq \left(\frac{e}{m}\right)_E e^{-i\lambda_{dE}}\frac{(\overline{\omega}_d/\omega_{0r})}{\overline{\omega}_d - \omega_0} J_0\mathcal{J}_{E0}\overline{\delta\phi_0}Q(F_0 + \delta g_{zA}). \quad (48)$$

Here, as in Sec. III A, $\lambda_{dE} = \boldsymbol{k}_\perp \cdot \boldsymbol{\rho}_d$, represents the finite banana-width effect and $\mathcal{J}_{E0} = \exp(i\lambda_{dE})$. Equation (47) then reduces to

$$\begin{aligned}\mathbb{I}\mathrm{m}\delta W_{k0A} = &\left(\frac{e^2}{m}\right)_E\left(\frac{\pi}{\omega_{0r}}\right)\int d^3\boldsymbol{X}\Big\langle J_0^2\mathcal{J}_{E0}^2\left|\overline{\delta\phi_0}\right|^2\overline{\omega}_d^2 \\ &\times\delta(\overline{\omega}_d - \omega_0)Q(F_0 + \delta g_{zA})_E\Big\rangle_v, \\ \equiv &\ \mathbb{I}\mathrm{m}\delta W_k^l + \mathbb{I}\mathrm{m}\delta W_{kz}^A,\end{aligned} \quad (49)$$

where δW_k^l and δW_k^A correspond to contributions to the instability drive due to, respectively, F_0 and δg_{zA}. Noting $|\omega_0| \ll |\omega_{*iE}|$, $Q \approx \hat{\omega}_* = (\boldsymbol{k}\times\boldsymbol{b}_0/\Omega)\cdot\hat{\boldsymbol{r}}\partial/\partial r$, and considering the resonance, $\omega_{0r} = \overline{\omega}_d(r_m|_{\varepsilon,\mu})$, where $q(r_m) = q_{\min}$ and $|\delta\phi_0|^2$ peaks at r_m, we then have, taking ω_{0r} and $\overline{\omega}_d > 0$, $\partial F_0/\partial r|_{r_m} < 0$ and, thus, $\hat{\omega}_* F_0 > 0$; i.e., $\mathbb{I}\mathrm{m}\delta W_k^l > 0$. This is, of course, just the usual trapped EP linear instability drive via the precessional resonance and $\partial F_0/\partial r < 0$ expansion free energy.

Following the same argument, we can consider $\mathbb{I}\mathrm{m}\delta W_{kz}^A$ due to $Q\delta g_{zA} \simeq \hat{\omega}_*\delta g_{zA}$. Note, as remarked earlier, δg_{zA} is given by the coupled Eqs. (43) and (44); involving an infinite sum of perturbation expansions; i.e., the Dyson-like equation. In the linear phase, however, we need only keep the first-order perturbation; i.e., dropping δg_{zA} in Eq. (48). Noting $\omega_0 = \omega_{0r} + i\gamma_0$ with γ_0 being the linear growth rate, and substituting Eq. (48) without δg_{zA} into Eq. (44), we can straightforwardly derive, near wave-particle resonance [22],

$$\delta g_{zA} \simeq \mathcal{J}_{zE}^2\mathcal{J}_{E0}^2\left|\frac{c}{B_0}\frac{n_0 q}{r}\frac{\overline{\omega}_d}{\omega_{0r}}\right|^2\frac{\partial}{\partial r}\frac{\left|\overline{\delta\phi_0}\right|^2}{(\overline{\omega}_d - \omega_{0r})^2 + \gamma_0^2}\frac{\partial F_0}{\partial r}. \quad (50)$$

In deriving Eq. (50), we have noted $\delta g_{zA} \propto \exp(2\gamma_0 t)$. Taking resonance near r_m such that $(\overline{\omega}_d - \omega_{0r})^2 \simeq \overline{\omega}_d'^2(r - r_m)^2$ and noting $\partial F_0/\partial r|_{r_m} < 0$, we, thus, have a hole $(\delta g_{zA} < 0)$ for $r < r_m$ and a clump $(\delta g_{zA} > 0)$ for $r > r_m$; consistent with the simulation result shown in Fig. 4. Consequently, $\partial\delta g_{zA}/\partial r|_{r_m} > 0$ and $\mathbb{I}\mathrm{m}\delta W_{kz}^A < 0$; i.e., δg_{zA}, as is well known, reduces the instability drive.

(Case B) Full ZFs in EP. In this case, δF_{g0B} and δF_{gzB} satisfy, respectively, Eqs. (40) and (41). Applying Eq. (39), the corresponding δg_{g0B} and δg_{zB} can then be shown to satisfy

$$\begin{aligned}(\mathcal{L}_g + \delta\mathcal{L}_{zX})\,\delta g_{g0B} = &i\left(\frac{e}{m}\right)Q\,(F_{g0} + \delta g_{zB}) \\ &\times J_0\left(\delta\phi - \frac{v_\parallel\delta A_\parallel}{c}\right)_0,\end{aligned} \quad (51)$$

$$\delta g_{zB} = \delta g_{zA} + \delta g_z^{(1)}, \quad (52)$$

where

$$\mathcal{L}_g\delta g_z^{(1)} = -\left(\frac{e}{m}\right)\frac{\partial F_0}{\partial\varepsilon}\frac{\partial}{\partial t}J_z\left(\delta\phi - \frac{v_\parallel\delta A_\parallel}{c}\right)_z, \quad (53)$$

and δg_{zA} given by Eq. (44). As in Case A, we can follow Eq. (45) to extract the compressional component of δg_{g0B}, δK_{0B};

$$(\mathcal{L}_g + i\omega_z)\,\delta K_{0B} = i\left(\frac{e}{m}\right) J_0 \frac{(\omega_d+\omega_z)}{\omega_{0r}} \delta\phi_0 Q(F_0+\delta g_{zB}). \tag{54}$$

$\mathbb{I}\mathrm{m}\delta W_{k0}$, Eq. (34), meanwhile, becomes

$$\mathbb{I}\mathrm{m}\delta W_{k0B} = e_E \mathbb{I}\mathrm{m}\int d^3\boldsymbol{X}\left\{\delta\phi_0^*\left\langle (J_0\omega_z+\omega_d J_0)\,\delta K_{0B}\right\rangle_v\right\}. \tag{55}$$

Again, taking trapped EP as an illustration, we have

$$\delta K_{0B} \simeq \left(\frac{e}{m}\right)_E e^{-i\lambda_{dE}} \frac{(\overline{\omega}_d+\omega_{zE})}{\overline{\omega}_d-\omega_0+\omega_{zE}} J_0 \mathcal{J}_{E0}\overline{\delta\phi_0} Q(F_0+\delta g_{zB}), \tag{56}$$

and

$$\mathbb{I}\mathrm{m}\delta W_{k0B} = \left(\frac{e^2}{m}\right)_E \frac{\pi}{\omega_{0r}} \int d^3\boldsymbol{X}\Big\langle J_0^2\mathcal{J}_{E0}^2|\overline{\delta\phi_0}|^2(\overline{\omega}_d+\omega_{zE})^2 \cdot \delta(\overline{\omega}_d-\omega_0+\omega_{zE})Q(F_0+\delta g_{zB})_E\Big\rangle_v. \tag{57}$$

Here, $\omega_{zE} = \overline{(c/B_0)\langle\delta \boldsymbol{E}_z\rangle \times \boldsymbol{b}_0\cdot\boldsymbol{k}_{\perp 0}}$. ZFs, thus, introduce two effects on the EP excitation of the instability. First, noting $|\omega_{zE}| \sim \mathcal{O}(\gamma_L) \ll |\omega_0|, |\overline{\omega}_d|$, $\delta\boldsymbol{E}_z$ introduces a small shift in the wave-particle resonance condition in the EP phase space; and, typically a negligible effect on the instability drive. We remark, however, ω_{zE} could play a more significant role in the nonlinear saturation process via the resonance detuning due to the finite $\partial\omega_{zE}/\partial r$ shearing relative to $\partial\overline{\omega}_d/\partial r$ [38]. The other effect, noting Eq. (52), is via the ZFs-induced phase-space structure, $\delta g_z^{(1)}$ given by Eq. (53). As in case (A), taking the resonance at r_m where $|\delta\phi_0|^2$ peaks, the additional drive then depends on $(\partial\delta g_z^{(1)}/\partial r)|_{r_m}$. Following the analysis in Sec. III A for the thermal ions, we have, for the trapped EPs [c.f. Eq. (26)],

$$\delta g_{zE}^{(1)} \simeq -\left(\frac{e}{m}\frac{\partial F_0}{\partial\varepsilon}\right) J_z \mathcal{J}_{Ez0}(\mathcal{J}_{Ez0}\Phi - \mathcal{J}_{Ez1}A)_z. \tag{58}$$

Here, we recall $\mathcal{J}_{Ez0} = \overline{\exp(i\lambda_{dEz})}$, $\lambda_{dEz} = \rho_{dr}k_{zr}$, and $\mathcal{J}_{Ez1} = \overline{(v_\parallel/c)\exp(i\lambda_{dEz})}$. Hence, for $|\lambda_{dEz}| < 1$, $\mathcal{J}_{Ez0} \simeq 1$, and $\mathcal{J}_{Ez1} \approx i\frac{v}{c}\rho_{bE}k_{zr} \propto \partial/\partial r$. Noting, from Eqs. (29) and (31), both Φ_z and A_z beat driven by RSAE are odd functions with respect to $(r - r_{\min})$, we then obtain

$$\left(\frac{\partial\delta g_{zE}^{(1)}}{\partial r}\right)\Bigg|_{r_m} \simeq -\left(\frac{e}{m}\frac{\partial F_0}{\partial\varepsilon}\right)\mathcal{J}_{Ez0}^2 \frac{\partial\Phi_z}{\partial r}\Bigg|_{r_m} \simeq -\left(\frac{e}{m}\frac{\partial F_0}{\partial\varepsilon}\right)\frac{c}{B_0}\frac{(1+c_0\eta_i)}{\omega_{0r}^2}k_{\theta 0}\omega_{*in}\frac{\partial^2}{\partial r^2}|\delta\phi_0|^2\Bigg|_{r_m} < 0. \tag{59}$$

Here, we note $\partial F_0/\partial\varepsilon < 0$ and $\partial^2|\delta\phi_0|^2/\partial r^2 < 0$ at r_m. That is, the additional $\delta\phi_z$ − induced EP phase-space structure, $\delta g_z^{(1)}$, further enhances the linear instability drive due to $\partial F_0/\partial r < 0$ and, hence, is destabilizing. One, thus, expects that the present Case B with ZFs in the EP dynamics will lead to a higher saturation level than the Case A without ZFs in the EP dynamics. This analytical prediction is consistent with the simulation results presented in Sec. II.

Case (C) Partial ZFs in EP. In this case, we suppress the ZFs in the EP gyro-center propagator; while keeping the ZFs-induced perturbed distribution. That is, Eq. (40) becomes

$$\mathcal{L}_g\delta F_{g0C} = -(\delta\mathcal{L}_{0X}+\delta\mathcal{L}_{0\varepsilon})(F_{g0}+\delta F_{gzC}). \tag{60}$$

Noting Eq. (39), Eq. (60) then leads to

$$\mathcal{L}_g\delta g_{g0C} = i\left(\frac{e}{m}\right)Q(F_{g0}+\delta F_{gzC})J_0\left(\delta\phi - \frac{v_\parallel\delta A_\parallel}{c}\right)_0. \tag{61}$$

Meanwhile, from Eq. (41) and noting $\delta\mathcal{L}_{zE}$ given by Eq. (37), we find

$$\begin{aligned}\delta F_{gzC} &= \left(\frac{e}{m}\right)\frac{\partial F_0}{\partial\varepsilon}J_0\delta\phi_z + \delta g_{zB}\\ &= \left(\frac{e}{m}\right)\frac{\partial F_0}{\partial\varepsilon}J_0\delta\phi_z + \delta g_{zA} + \delta g_z^{(1)},\end{aligned} \tag{62}$$

where δg_{zA} and $\delta g_z^{(1)}$ are given, respectively, by Eq. (44) and Eq. (53). From Eq. (61), the compressional component, δK_{0C}, obeys

$$\mathcal{L}_g\delta K_{0C} = i\left(\frac{e}{m}\right)J_0\frac{\omega_d}{\omega_{0r}}Q(F_{g0}+\delta F_{gzC})\delta\phi_0, \tag{63}$$

and $\mathbb{I}\mathrm{m}\delta W_{k0C}$ becomes

$$\mathbb{I}\mathrm{m}\delta W_{k0C} = e_E\mathbb{I}\mathrm{m}\int d^3\boldsymbol{X}\{\delta\phi_0^*\langle\omega_d J_0\delta K_{0C}\rangle_v\}. \tag{64}$$

Considering only the trapped EPs, we have

$$\delta K_{0C} \simeq \left(\frac{e}{m}\right)e^{-i\lambda_{dE}}\frac{\overline{\omega}_d}{\overline{\omega}_d-\omega_0}\mathcal{J}_{E0}J_0\overline{\delta\phi_0}Q(F_{g0}+\delta F_{gzC}). \tag{65}$$

$\mathbb{I}\mathrm{m}\delta W_{k0C}$ is then further reduced to

$$\mathbb{I}\mathrm{m}\delta W_{k0C} = \left(\frac{e^2}{m}\right)_E\frac{\pi}{\omega_{0r}}\int d^3\boldsymbol{X}\Big\langle J_0^2\mathcal{J}_{E0}^2|\overline{\delta\phi_0}|^2\overline{\omega}_d^2\delta(\overline{\omega}_d-\omega_0) \cdot Q(F_{g0}+\delta F_{gzC})\Big\rangle_v. \tag{66}$$

Equations (62) and (66) indicate that, relative to the Full-ZFs Case B, the present Partial-ZFs Case C introduces an additional EP PSZS, $(e/m)(\partial F_0/\partial\varepsilon)J_0\delta\phi_z$. The corresponding instability drive at r_m is then given by

$$\frac{\partial}{\partial r}\left[\left(\frac{e}{m}\right)\left(\frac{\partial F_0}{\partial\varepsilon}\right)J_0\delta\phi_z\right]\Bigg|_{r_m} \simeq \frac{e}{m}\frac{\partial F_0}{\partial\varepsilon}\frac{\partial\delta\phi_z}{\partial r}\Bigg|_{r_m} > 0. \tag{67}$$

That is, suppressing the zonal drift-shearing in the EP gyro-center propagator, in fact, provides stabilization with respect to the Full-ZFs Case B; which is consistent with simulation reported in Sec. II. Compared to the No-ZFs Case A, Eq. (62) indicates that the additional EP

PSZS is given by $(e/m)(\partial F_0/\partial\varepsilon)J_z\delta\phi_z + \delta g_z^{(1)}$. Noting Eq. (59) and Eq. (31), the additional instability drive relative to Case A is, thus,

$$\begin{aligned}&\frac{\partial}{\partial r}\left[\left(\frac{e}{m}\right)_E \frac{\partial F_0}{\partial \varepsilon} J_z(1-\mathcal{J}_{E0}^2)\Phi_z\right]\Big|_{r_m}\\ &\approx \left(\frac{e}{m}\right)_E \left(\frac{\partial F_0}{\partial \varepsilon}\right)\frac{c}{B_0}\frac{(1+c_0\eta_i)}{\omega_{0r}^2}k_{\theta 0}\omega_{*in}(1-\mathcal{J}_{E0}^2)\frac{\partial^2}{\partial r^2}\left|\delta\phi_0\right|^2\Big|_{r_m}\\ &> 0;\end{aligned} \tag{68}$$

i.e., Case C with the zonal drift-shearing suppressed is, qualitatively, more stable than the No-ZFs Case A. Quantitatively, for $|k_{rz}\rho_{dE}| < 1$, $1-\mathcal{J}_{E0}^2 \simeq (k_{zr}\rho_{dE})^2 \ll 1$, the additional stabilization is negligibly small. Case C, therefore, essentially coincides with Case A, and this analytical result is consistent with the simulation result presented in Sec. II.

IV. CONCLUSIONS AND DISCUSSIONS

In summary, we have employed nonlinear gyrokinetic simulation as well as analytical theory to investigate the effects of ZFs on the EP's drive of RSAE instability. We have derived analytical expressions for the ZFs beat-driven by RSAE; which are in good agreement with the simulation results. Three cases of GTC simulations with various terms of ZFs in the EP gyrokinetic equation turned on and off are then carried out. The results, contrary to the usual expectation, indicate that ZFs tend to enhance EP's drive and, thereby, increase the saturation level. Corresponding analytical theory is also developed; which demonstrates that, in each case, the ZFs-induced EP phase-space zonal structures are different, and this, according to the general fishbone-like dispersion relation, gives rise to, consistent with simulation results, the additional stabilization/destabilization by ZFs. We note that, while this work is focused on the RSAE, it will be interesting to carry out a corresponding study on TAE and investigate if ZFs have similar effects on the EP drive.

As we remark in Sec. I, it has been well established that ZFs tends to suppress RSAE to a significantly lower saturation level. Our current results, however, indicate that such suppression is not due to ZFs effects on EP; i.e., not via the second route. Thus, one must conclude that ZFs suppress RSAE mainly via the channel of nonlinear physics of thermal plasma; i.e., the first route. It will, therefore, be interesting to employ, again, both nonlinear simulation and analytical theory, to investigate the detailed nonlinear mechanisms of thermal plasmas which could suppress the RSAE. This will be a subject of future investigations.

Acknowledgments

This work has been supported in part by the National key R&D Program of China under Grant No. 2022YFE03040002, the National Science Foundation of China under Grant Nos. 12175053, 12261131622 and 1205508, the Italian Ministry of Foreign Affairs with Grant No. CN23GR02, the Strategic Priority Research Program of the Chinese Academy of Sciences (Grant No. XDB0500302), and the start-up funding of Institute of Physics, Chinese Academy of Sciences under Grant No. E3CB031R21. This work has also partly been carried out within the framework of the EUROfusion Consortium, funded by the European Union via the Euratom Research and Training Programme (Grant Agreement No 101052200−EUROfusion). Views and opinions expressed are however those of the author(s) only and do not necessarily reflect those of the European Union or the European Commission. Neither the European Union nor the European Commission can be held responsible for them.

References

[1] H. Kimura, Y. Kusama, M. Saigusa, G. J. Kramer, K. Tobita, M. Nemoto, T. Kondoh, T. Nishitani, O. D. Costa, T. Ozeki, et al., Nucl. Fusion **38**, 1303 (1998).
[2] S. E. Sharapov, D. Testa, B. Alper, D. N. Borba, A. Fasoli, N. C. Hawkes, R. F. Heeter, M. Mantsinen, M. G. V. Hellermann, and the EFDA-JET work programme, Phys. Lett. A **289**, 127 (2001).
[3] Y. Chen, G. Fu, C. Collins, S. Taimourzadeh, and S. Parker, Phys. Plasmas **25**, 032304 (2018).
[4] T. Wang, S. Wei, S. Briguglio, G. Vlad, F. Zonca, and Z. Qiu, Plasma Sci. Technol. **26**, 053001 (2024).
[5] P. Liu, X. Wei, Z. Lin, G. Brochard, G. Choi, and J. Nicolau, Rev. Mod. Plasma Phys. **7**, 15 (2023).
[6] S. Wei, T. Wang, N. Chen, and Z. Qiu, J. Plasma Phys. **87**, 905870505 (2021).
[7] F. Zonca and L. Chen, Phys. Plasmas **21**, 072120 (2014).
[8] F. Zonca and L. Chen, Phys. Plasmas **21**, 072121 (2014).
[9] F. Zonca, L. Chen, S. Briguglio, G. Fogaccia, G. Vlad, and X. Wang, New J. Phys. **17**, 013052 (2015).
[10] Z. Lin, T. Hahm, W. Lee, W. Tang, and R. White, Science **281**, 3 (1998).
[11] C. Collins, W. Heidbrink, M. Austin, G. Kramer, D. Pace, C. Petty, L. Stagner, M. V. Zeeland, R. White, Y. Zhu, et al., Phys. Rev. Lett. **116**, 095001 (2016).
[12] L. L. Lao, H. S. John, and R. D. Stambaugh, Nucl. Fusion **25**, 1611 (1985).
[13] S. Taimourzadeh, E. Bass, Y. Chen, C. Collins, N. Gorelenkov, A. Knies, Z. Lu, D. Spong, Y. Todo, M. Austin, et al., Nucl. Fusion **59**, 066006 (2019).
[14] I. Holod, W. Zhang, Y. Xiao, and Z. Lin, Phys. Plasmas **16**, 122307 (2009).
[15] A. J. Brizard and T. S. Hahm, Rev. Mod. Phys. **79**, 421 (2007).
[16] S. E. Parker and W. W. Lee, Phys. Fluids B **5**, 77 (1993).

[17] T. Wang, Z. Qiu, F. Zonca, S. Briguglio, and G. Vlad, Nucl. Fusion **60**, 126032 (2020).
[18] E. A. Frieman and L. Chen, Phys. Fluids B **25**, 502 (1982).
[19] M. V. Falessi, L. Chen, Z. Qiu, and F. Zonca, New J. Phys. **25**, 123035 (2023).
[20] M. N. Rosenbluth and F. L. Hinton, Phys. Rev. Lett. **80**, 724 (1998).
[21] C. Z. Cheng, L. Chen, and M. S. Chance, Ann. Phys. **161**, 21 (1985).
[22] L. Chen and F. Zonca, Rev. Mod. Phys. **88**, 015008 (2016).
[23] D. Spong, E. Bass, W. Deng, W. Heidbrink, Z. Lin, B. Tobias, M. V. Zeeland, M. Austin, C. Domier, and J. N.C. Luhmann, Phys. Plasmas **19**, 082511 (2012), ISSN 1070-664X.
[24] Y. Todo, H. Berk, and B. Breizman, Nucl. Fusion **52**, 033003 (2012).
[25] J. Zhu, Z. Ma, and S. Wang, Phys. Plasmas **23**, 122506 (2016), ISSN 1070-664X.
[26] T. O'Neil, Phys. Fluids **8**, 2255 (1965).
[27] H. Zhang, Z. Lin, and I. Holod, Phys. Rev. Lett. **109**, 025001 (2012).
[28] H. Zhang, Z. Lin, W. Deng, I. Holod, Z. Wang, Y. Xiao, and W. Zhang, Phys. Plasmas **20**, 012510 (2013), ISSN 1070-664X.
[29] J. Zhu, G. Y. Fu, and Z. W. Ma, Phys. Plasmas **20**, 072508 (2013).
[30] S. Briguglio, X. Wang, F. Zonca, G. Vlad, G. Fogaccia, C. D. Troia, and V. Fusco, Phys. Plasmas **21**, 112301 (2014).
[31] S. Briguglio, M. Schneller, X. Wang, C. D. Troia, T. Hayward-Schneider, V. Fusco, G. Vlad, and G. Fogaccia, Nucl. Fusion **57**, 072001 (2017).
[32] F. Zonca, S. Briguglio, L. Chen, G. Fogaccia, and G. Vlad, Nucl. Fusion **45**, 477 (2005).
[33] F. Zonca, P. Buratti, A. Cardinali, L. Chen, J.-Q. Dong, Y.-X. Long, A. Milovanov, F. Romanelli, P. Smeulders, L. Wang, et al., Nucl. Fusion **47**, 1588 (2007).
[34] F. Zonca, L. Chen, S. Briguglio, G. Fogaccia, A. V. Milovanov, Z. Qiu, G. Vlad, and X. Wang, Plasma Phys. Control. Fusion **57**, 014024 (2015).
[35] H. L. Berk, B. N. Breizman, and H. Ye, Phys. Rev. Lett. **68**, 3563 (1992).
[36] X. Wang, H. Wang, Y. Todo, Y. Xu, J. Wang, H. Liu, J. Huang, X. Zhang, H. Liu, J. Cheng, et al., Plasam Phys. Control. Fusion **63**, 015004 (2021).
[37] L. Chen and A. Hasegawa, J. Geophys. Res. **96**, 1503 (1991).
[38] G. Brochard, C. Liu, X. Wei, W. Heidbrink, Z. Lin, N. Gorelenkov, C. Chrystal, X. Du, J. Bao, A. R. Polevoi, et al., Phys. Rev. Lett. **132**, 075101 (2024).